JOURNAL OF MATERIALS SCIENCE 7 (1972) 485–493

Grinding Forces and the Machining of Magnesium Oxide Crystals

B. G. KOEPKE, R. J. STOKES
Honeywell Inc., Corporate Research Center, 500 Washington Avenue South, Hopkins, Minnesota, USA

The forces acting on magnesium oxide crystals during a surface grinding operation have been studied as a function of rate of material removal and crystal orientation, using two different conventional grinding wheels.

The results are discussed in terms of the resulting surface and subsurface damage and the geometry of the wheel-workpiece interaction. The results are consistent with the observations that chip formation occurs by plastic flow under a 46-grit alumina wheel, while material is removed completely by brittle fracture under a 100-grit diamond wheel. It is demonstrated that the stress on an individual chip is within an order of magnitude of the theoretical shear strength of the workpiece, thus accounting for the presence of both surface and subsurface plastic deformation.

1. Introduction

Recently, considerable interest has arisen in the fundamental aspects of ceramic machining, particularly with respect to understanding the nature and extent of damage introduced into the ceramic workpiece [1, 2]. It has been shown that the damage is twofold: first, brittle fracture and cracking is introduced into the surface, and second, subsurface plastic deformation occurs with the consequent dislocation arrays [3-5] and residual stresses.

In order to understand the mechanisms by which damage is introduced, conditions at the tool-workpiece interface must be defined. This is a difficult problem due to the high cutting speeds involved. Rough estimates indicate strain rates of the order of 10^6 sec^{-1}. These are strain rates at which stress waves play a significant role in the impact fracture of a chip [6].

To get some quantitative measurements concerning the phenomena occurring we have studied the forces involved in removing material by surface grinding. The measurement of grinding forces and their use in studying the mechanisms of chip formation have been reported in depth for metals [7-9], but only recently have similar studies been attempted on ceramics, the most notable of these with a single-point cutting tool [6].

This paper analyses measurements of grinding forces using conventional grinding wheels and magnesium oxide single crystals. Magnesium oxide crystal have been previously characterised for grinding damage using different grinding wheels, and the mechanism of material removal has been identified [3]. By correlating the grinding force measurements with surface damage for crystals of varying orientation, we have been able to develop a better understanding of the processes of chip formation in ceramics.

2. Experimental Procedure

The specimens for these studies were magnesium oxide single crystals which had been cleaved into rectangular slabs with approximate dimensions 1.2 × 0.6 × 0.3 cm. They were cemented onto flat steel plates and held in a vice attached to a grinding dynamometer based on a design by Marshall and Shaw [7].

The dynamometer was arranged to measure (with strain gauges), the average vertical and horizontal forces acting on the workpiece during grinding. These forces were measured independently.

The sensitivity of the dynamometer was adjusted to the point where the smallest resolvable vertical force was 30 g and the smallest resolvable horizontal force was 5 g. Repeated calibrations showed the output to be linear and reproducible to within 10%.

Grinding was carried out with a DoAll Model D618-7 high speed precision surface grinder having a fixed spindle speed of 3540 rpm. Both the depth of cut, d, and the workpiece feed rate, v, were varied during the experiments. Two wheels were used for grinding, a 46-grit vitrified-bond alumina wheel (Norton Type AA-46-M8-V40) and 100-grit resinoid-bond diamond wheel (DoAll Type D1A1-MD100N1DOB1/4B3). The cutting face of the alumina wheel is relatively open and contains voids, whereas the diamond wheel is closed and consists of diamond grains protruding from the continuous matrix. Photomicrographs of the wheel surfaces were included in an earlier paper [3]. All grinding was carried out dry.

In a typical experiment a given single crystal sample was ground at a number of different machine settings (i.e. varying d and v) so that data could be obtained from a single specimen. To be consistent, certain precautions were taken before each run; the alumina wheel was dressed every time the work-piece feed rate and/or depth of cut was changed, and the sequence of experiments was always toward higher rates of material removal; the diamond wheel was dressed with a silicon carbide wheel only once at the beginning of a series of experiments. At least three measurements were taken for each combination of feed rate and depth of cut.

In the present work magnesia crystals were always machined over {100} planes, but the direction was varied from ⟨100⟩ by as much as 30 degrees. Following a grinding experiment, the samples were examined for surface and subsurface damage. Subsurface damage was revealed by the dislocation etching procedure and the surface damage by optical and scanning electron microscopy.

3. Results

3.1. Grinding Forces on Crystals machined over {100} Planes in ⟨100⟩ Directions

In the first series of tests the orientation of the magnesia crystals was fixed, and grinding was carried out on a {100} plane in a ⟨100⟩ direction. This orientation is the one most favourably oriented for plastic shear as will be demonstrated later. The horizontal and vertical grinding forces were measured as a function of the machining variables (depth of cut and workpiece feed rate) for the two wheels (alumina and diamond).

With the alumina wheel, both the horizontal and vertical grinding forces varied linearly with the feed rate for different depths of cut, as shown in fig. 1. Each data point is the average of six to nine measurements taken on three different crystals. The bars indicate the total scatter in the data. No bars are drawn where the data fell within the plotted symbol. The grinding forces with the alumina wheel also varied linearly with depth of cut for different feed rates.

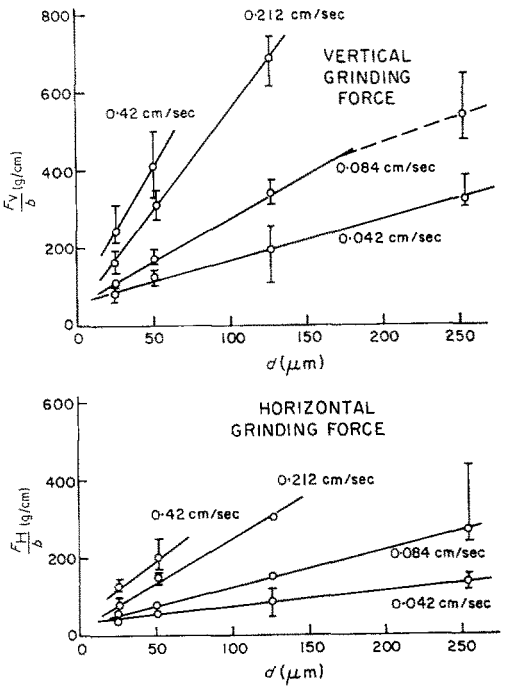

Figure 1 Vertical (F_V) and horizontal (F_H) grinding forces on crystals ground on {100} faces in ⟨100⟩ directions dry with a 46-grit alumina wheel plotted at various depths of cut as a function of feed rate (v) (b is the width of the cut; each data point represents the average of six to nine grinding passes).

When crystals were ground with the diamond wheel the results were very different. Fig. 2 shows the variation of the horizontal and vertical grinding forces as a function of the feed rate for different depths of cut with the 100-grit diamond wheel. Note first that the horizontal grinding forces are low and are essentially independent of the rate of material removal (except for 127 μm cuts at high feed rates). Second, the vertical grinding forces are very much higher than those experienced with the alumina wheel and do not

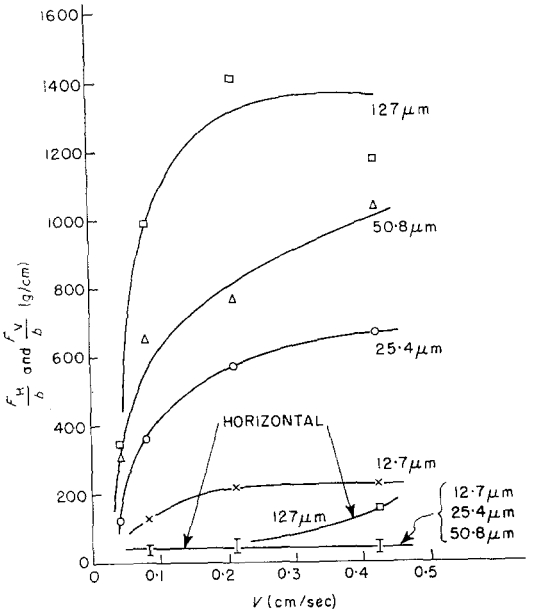

Figure 2 Vertical (F_V) and horizontal (F_H) grinding forces at various depths of cut as a function of workpiece feed rate for magnesium oxide crystals ground in the {100} ⟨100⟩ orientation dry with a 100-grit diamond wheel (*b* is the width of the cut).

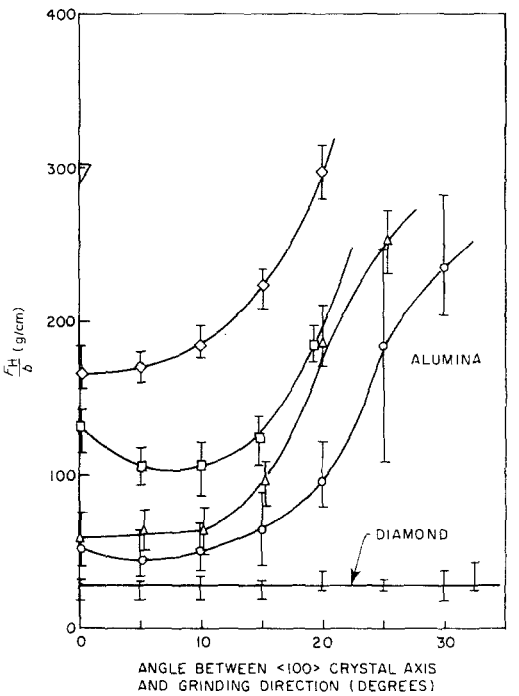

Figure 3 Tangential grinding force as a function of the angle between the ⟨100⟩ crystal axis and the grinding direction for magnesium oxide crystals ground dry on {100} faces with a 46-grit alumina and a 100-grit diamond wheel at various material removal rates (46-grit alumina wheel: ○, $d = 25.4$ μ, $v = 0.042$ cm/sec; △, $d = 25.4$ μ, $v = 0.21$ cm/sec; □, $d = 25.4$ μ, $v = 0.42$ cm/sec; ◇, $d = 50.8$ μ, $v = 0.42$ cm/sec; ▽, $d = 12.7$ μ, $v = 0.21$ cm/sec; 100-grit diamond wheel: I, $d = 25.4$ μ, $v = 0.042$ cm/sec and 0.21 cm/sec).

vary linearly with the rate of material removal, but approach an asymptotic value.

3.2. Grinding Forces on Crystals machined over {100} Planes in varying Directions

To gain further insight into the mechanism of chip formation and material removal, the direction of grinding was changed gradually away from ⟨100⟩. Both alumina and diamond grinding wheels were used, and the depth of cut and feed rate were varied as before.

With the alumina wheel, changing the grinding direction had a drastic effect on the horizontal grinding force as shown for different material removal rates in fig. 3. Up to 10 degrees from ⟨100⟩, the horizontal force remained essentially constant (with maybe a slight decrease in some instances), but above 10 degrees the horizontal grinding forces increased rapidly to the point where the crystals shattered without machining for a 30-degree orientation. The vertical grinding forces varied with orientation in about the same manner as the horizontal grinding forces.

With the diamond wheel, the horizontal grinding forces were low and independent of orientation, as shown by the lower curve on fig. 3. Note that these specimens could be machined at any angle without shattering. The vertical grinding forces plotted in fig. 4 showed a greater sensitivity to the orientation, and in addition were sensitive to material removal rate as noted earlier in fig. 2. To summarise these observations:

(i) The difference in tool-workpiece interaction using alumina and diamond grinding wheels shows up quite dramatically using grinding force measurements.

(ii) Using an alumina wheel, the horizontal grinding forces vary linearly with the rate of material removal and are very sensitive to orientation. Using a diamond wheel, the horizontal grinding forces are low and independent of rate of material removal or orientation.

(iii) Using an alumina wheel, the vertical grinding forces vary linearly with the rate of material

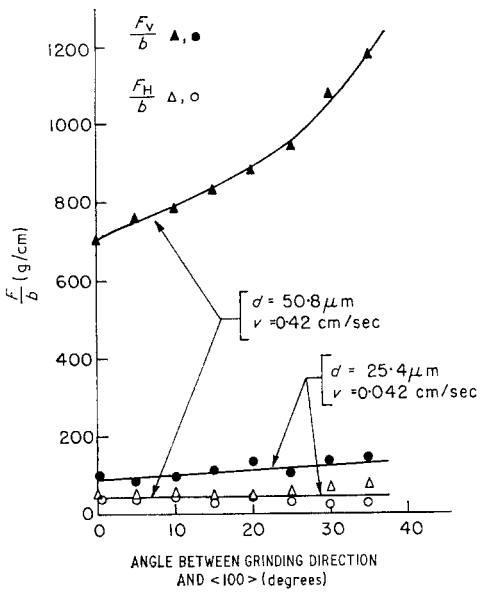

Figure 4 Vertical and horizontal grinding forces measured on {100} magnesium oxide crystal faces as a function of the angle that the grinding direction makes with ⟨100⟩; data are shown for crystals ground dry with a 100-grit diamond wheel at two rates of material removal.

removal and are very sensitive to orientation. Using a diamond wheel, the vertical grinding forces are extremely sensitive to the rate of material removal and slightly sensitive to orientation.

3.3. Surface and Subsurface Damage

The differences in grinding forces observed when samples are machined with the alumina or the diamond wheel are reflected by differences in the respective surface finishes. These differences have already been described [3, 4], but we will mention them again here briefly for completeness.

When magnesium oxide crystals are ground with the 46-grit alumina wheel on the dynamometer, the rate at which the wheel can expel swarf is less than the rate of material removal. In this case, fresh cutting points on the wheel surfaces are prevented from impacting the workpiece, and material is removed almost exclusively by plastic flow. The resulting burnished surface is quite smooth and contains, in many instances, shallow {100} cracks that result from thermal stresses set up when the hot, as-ground surface is quenched following passage of the wheel.

When magnesium oxide crystals are ground with the 100-grit diamond wheel, a much different type of surface is produced. The surface of the diamond wheel is closed. As a result, the wheel does not load up, and fresh cutting points always impact the surface of the crystal. Chip formation in this case occurs almost entirely by brittle fracture, producing rough surfaces containing fractures lying predominantly on {100} planes.

Differences in the subsurface damage introduced in magnesium oxide crystals by the 46-grit alumina and 100-grit diamond wheels has also been reported elsewhere [3, 4], and will be reviewed only briefly at this time. When machined crystals are cleaved on {100} faces transverse to the ground surface and etched, the subsurface damage is revealed on the cleaved surface as a dense band of dislocation etch pits adjacent to the ground surface.

The plastically deformed layer in crystals ground with the alumina wheel is usually discrete, and very little slip is observed penetrating the dense surface layer until high rates of material removal are reached. The depth of damage varies from 30 to over 200 μm as the rate of material removal is increased. The damage layer in crystals ground with the diamond wheel, on the other hand, is not of constant depth and slip bands penetrating the dense surface layer are generally observed at even low rates of material removal. The depth of damage in crystals ground with the diamond wheel is usually 40 to about 100 μm deep and does not vary sensibly with the rate of material removal. The scatter in the measured depth of damage results from the uneveness of the damage layer. In summary:

(i) Grinding with the alumina wheel produced smooth burnished surfaces under all conditions, whereas the diamond wheel produced a rough surface containing large amounts of cleavage fracture under all conditions.

(ii) Both wheels introduced a plastically deformed layer underneath the ground surface. The damage produced by the diamond wheel was not as discrete as that produced by the alumina wheel, and its depth did not vary in a regular fashion with the rate of material removal. The depth of damage in crystals ground with the alumina wheel increased with the rate of material removal.

4. Discussion Results

The above results and an earlier study [3] have shown that the grinding forces and the surface condition resulting from a given ceramic machining operation are quite sensitive to the wheel

workpiece combination. The correlation between these two parameters will be discussed later. First, it is useful to extend the grinding force measurements to estimate the energy expended during chip removal and the magnitude of the stress on a single chip. To do this we must first define and measure certain grinding geometry parameters.

4.1. Grinding Geometry

It is necessary to consider the geometry of chip formation, i.e. what is the size and shape of an individual chip, and how is this size related to grinding parameters such as the distribution of cutting points, the workpiece feed rate and wheel depth of cut.

The shape of an idealised grinding chip is represented by the dashed area in fig. 5. The workpiece moves forward a distance, PQ, in the time an abrasive grain on the wheel surface cuts the length of the chip. $PQSR$ is approximately triangular in shape as shown. The length, l, and maximum thickness, t, of the chip are given [8] in terms of determinable quantities, by

$$l = \sqrt{Dd} \tag{1}$$

and

$$t = \left[\frac{4v}{\pi cnrd}\sqrt{\frac{d}{D}}\right]^{\frac{1}{2}} \tag{2}$$

where D = wheel diameter, d = wheel depth of cut, v = workpiece feed rate, n = wheel speed in rpm, r = ratio of mean scratch width to mean scratch depth, and c = areal density of cutting points on the wheel surface. Values of c and r have been measured for the wheels used in this study by the techniques of Backer, *et al* [8] and are given below.

Wheel	$c(\text{cm}^{-2})$	r
46-grit alumina	300	15.2
100-grit diamond	480	1.6

The above measurements of r have brought out some important geometrical differences between a 46-grit alumina and a 100-grit diamond wheel. The ratio of the mean scratch width to mean scratch depth of the alumina wheel is 9.5 times that of the diamond wheel. In other words, the profile of the cutting faces of both wheels is completely different. The cutting face of the alumina wheel is composed of very shallow, wide abrasive points, while that of the diamond wheel is composed of high, sharp needle-like abrasives. This is shown schematically in fig. 6.

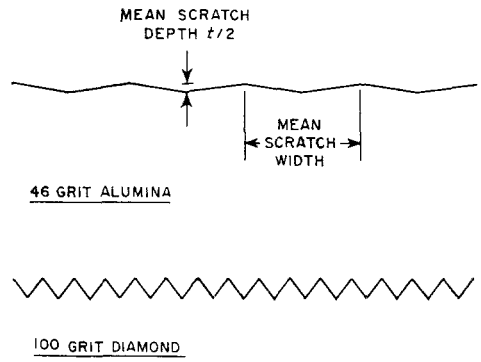

Figure 6 Schematic diagram showing the difference in the profiles of the cutting faces of the two grinding wheels used in this study.

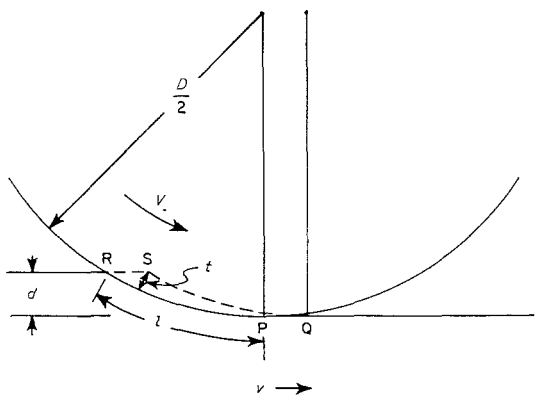

Figure 5 Schematic diagram showing the shape of an idealised grinding chip *PQSR* taken with a wheel depth of cut (d) and a workpiece feed rate (v); (t) is the maximum chip thickness and (l) is the chip length.

Values for l and r can be calculated as a function of machine setting using equations 1 and 2. Typical values are given below for both wheels.

d (μm)	v (cm/sec)	Wheel	t (μm)	l (mm)
25.4	0.042	46-grit alumina	0.12	2.1
		100-grit diamond	0.32	2.0
25.4	0.42	46-grit alumina	0.37	2.1
		100-grit diamond	1.0	2.0
50.8	0.42	46-grit alumina	0.43	3.0
		100-grit diamond	1.2	2.8

These values indicate that the actual depth to which an abrasive grain extends beyond a wheel surface (approximately equal to t) is only a fraction of its size. Furthermore, the maximum

chip thickness (also referred to as the grit depth of cut, t) varies with both wheel depth of cut, d, and feed rate, v, and, for the feeds and speeds used in this study, is on the order of $\frac{1}{4}$ to 1 μm. This is an extremely small number, two orders of magnitude less than the wheel depth of cut.

As expected from the geometry shown in fig. 5, the chip length is quite long in relation to its thickness, being on the order of 10^4 t. In other words, the production of a chip during surface grinding essentially involves making a long thin scratch. Note also that, even though the abrasive size is smaller, the grit depth of cut for the 100-grit diamond wheel is over twice that of the 46-grit alumina wheel. The chip lengths for both wheels are about the same. These observations are of value in understanding the difference in performance between the wheels.

4.2. Specific Grinding Energy

For the purposes of rationalising grinding measurements in metals, the concept of specific grinding energy (U) has been introduced [7]. This is defined as the energy expended in removing unit volume of material and is given by

$$U = \frac{\pi\, DnF_H}{vdb} \qquad (3)$$

where b is the width of the specimen and the other quantities in the equation have been defined earlier.

Fig. 7 plots the specific grinding energy as a function of the wheel depth of cut at various feed rates for magnesium oxide crystals ground with the alumina and diamond wheels. The energies are very high, indicating that grinding is an extremely inefficient process. Furthermore, as one would expect from equation 3, the energies increase as the wheel depth of cut and feed rate decrease. It should be noted that the specific grinding energies obtained with the alumina wheel are on the order of four times those obtained with the diamond wheel. Whether the higher energies under the alumina wheel reflect differences in mechanism of chip formation or cutting point geometry or both will be discussed later.

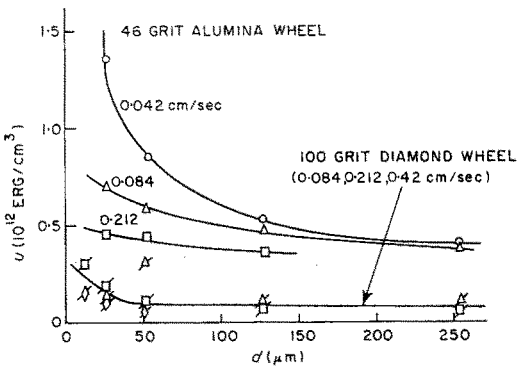

Figure 7 Specific grinding energy plotted at various feed rates as a function of depth of cut for magnesium oxide crystals ground with a 46-grit alumina and a 100-grit diamond wheel on {100} faces in ⟨100⟩ directions.

When the data of fig. 7 are replotted as a function of the grit depth of cut, t, equation 2, the results fall on a continuous curve as shown in fig. 8. The specific grinding energy appears to depend very strongly on the grit depth of cut and falls off rapidly as the chip thickness increases. The continuity from the alumina to the diamond wheel results is considered fortuitous for two reasons. First, the two wheels clearly have a different cutting point geometry (fig. 6), and the two wheels result in two different material removal mechanisms. Second, if the results for orientations other than ⟨100⟩, as illustrated in fig. 3, are considered, the specific grinding energy calculations for the alumina wheel are displaced upwards while the values for the diamond wheel remain constant, making a similar curve discontinuous.

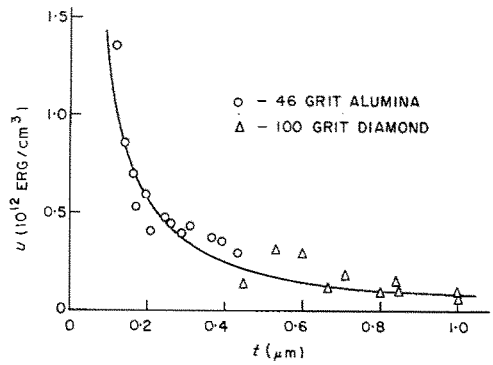

Figure 8 Specific grinding energies shown in fig. 7 replotted as a function of the grit depth of cut (t).

A similar strong dependence of the specific grinding energy on maximum chip thickness, t, has been found in cutting and grinding studies on metals [8, 9]. That work has shown that the specific grinding energy can be expressed by:

$$U = \frac{K}{t^n} \qquad (4)$$

where K and n are constants, and n is about

0.2 for metals. This same expression can be used to describe the data on the magnesium oxide crystals in this study. In fact, the line drawn through the data points in fig. 8 is given by the following expression:

$$U = \frac{1.35 \times 10^{12}}{t^{0.22}} \text{ erg/cm}^3.$$

Note that the value of n is very close to that obtained for metals suggesting a similarity in removal mechanisms.

4.3. The Relationship Between the Specific Grinding Energy and the Stress on a Single Chip

The stress on a single chip can be estimated in terms of the specific grinding energy and the grinding geometry by the following argument due to Backer [10, 11]. The work expended in unit time, $\dot{W}$, is equal to $Uvdb$, and the rate of chip formation, R, is equal to Vbc. Thus, the work expended in producing a single chip is $\dot{W}$ divided by R, and assuming the mean force on the chip to be the work divided by the chip length gives:

$$\bar{F}_{\text{chip}} = \frac{Uvd}{Vcl}. \tag{5}$$

The volume of a single chip is the rate of material removal divided by the rate of chip formation, i.e. vdb/Vbc, and its mean cross-sectional area is the volume divided by the chip length, i.e.

$$\bar{A}_{\text{chip}} = \frac{vd}{Vcl}. \tag{6}$$

Hence, the mean stress on the chip is

$$\sigma_{\text{chip}} = \frac{\bar{F}_{\text{chip}}}{\bar{A}_{\text{chip}}} = U. \tag{7}$$

This shows the mean stress on a chip to be approximated by the specific grinding energy, a relationship which attaches some significance to U. From figs. 7 and 8 these stresses are within an order of magnitude of the theoretical shear strength of magnesium oxide, i.e. $G/10$ where G is the shear modulus [12].

4.4. The Relationship between the Grinding Force and Machining Parameters.

The magnitude of grinding forces can be estimated by another energy balance approach [6]. In this analysis it is assumed that the kinetic energy imparted to the material in unit time is dispersed as strain energy in the machined workpiece. Other contributions to energy balance such as thermal effects and the kinetic energy of swarf are neglected.

The kinetic energy input to the workpiece in unit time is

$$\dot{E}_K = \tfrac{1}{2}\rho\, lvdbV^2$$

where ρ is the density of the workpiece material. Thus, in the time taken to cut a single chip, $\Delta t = l/V$, the kinetic energy input is

$$E_K = \tfrac{1}{2}\rho\, vdbV.$$

But this is spread over many chips, $bc^{\frac{1}{2}}$ in fact, whose area, $\bar{A}_{\text{chip}}$, is given by equation 6, so that the kinetic energy input per unit machined area is

$$\bar{E}_K = \tfrac{1}{2}\rho\, l^2\, V^2\, c^{\frac{1}{2}}. \tag{8}$$

The strain energy absorbed per unit machined area is the product of the strain energy per unit volume and the depth of damage, S; i.e.

$$\bar{E}_S = \bar{\sigma}_{\text{chip}}\, \bar{\epsilon}_{\text{chip}}\, S$$

where $\bar{\epsilon}_{\text{chip}}$ is the mean strain of the chip. Since magnesium oxide surfaces are burnished by plastic flow when machined with the alumina wheel, it is reasonable to assume that the relationship between stress ($\bar{\sigma}_{\text{chip}}$) and strain ($\bar{\epsilon}_{\text{chip}}$) is given by the conventional parabolic relation: [13]

$$\bar{\sigma}_{\text{chip}} = B\,(\bar{\epsilon}_{\text{chip}})^{\frac{1}{2}}$$

Thus,

$$E_S = \left(\frac{\bar{\sigma}_{\text{chip}}}{B^2}\right)^3 S \tag{9}$$

According to equation 7 the mean stress on a chip is equal to the specific grinding energy which is defined by equation 3. Substituting equation 3 in equation 9 gives,

$$\bar{E}_S = \left(\frac{\pi\, Dn\, F_{\text{H}}}{vdb}\right)^3 \frac{S}{B^2} \tag{10}$$

Assuming that kinetic energy input is equal to the strain energy absorbed, we equate equations 8 and 10 and solve for F_{H}/b. Using equation 1 and $V = \pi nD$ this gives

$$\frac{F_{\text{H}}}{b} = \left(\rho\, \frac{c^{\frac{1}{2}}\, DB^2}{2V}\right)^{1/3} \frac{vd^{4/3}}{S^{1/3}} \tag{11}$$

Note that this relationship predicts the grinding force to be proportional to both the feed rate, v, and the depth of cut, d ($\sim d^{4/3}$), consistent with the observations of fig. 1. It also predicts an inverse relationship between grinding force and

wheel speed, as experienced by Gielisse and Stanislao [6]. However, it also indicates an inverse relationship between grinding force and depth of damage which is contrary to what one would anticipate and to experimental results.

4.5. Grinding Forces and the Mechanism of Material Removal

As was pointed out earlier, the alumina wheel removes material by plastic flow and the diamond wheel by cleavage fracture. The difference in horizontal grinding forces between the two wheels and their dependence on machining parameters noted in figs. 1 to 4 illustrates the strong effect of frictional forces resulting from plastic flow.

In the case of the alumina wheel, the horizontal grinding force is proportional to the rate of material removal as predicted by equation 11. The short range stresses acting on the chip are within an order of magnitude of the theoretical shear strength, and the occurrence of plastic shear is, therefore, not surprising. These estimated stresses are extremely sensitive to the grit depth of cut (fig. 8) increasing as the cut gets smaller. The reason for this sensitivity is a size effect in that as the cut gets smaller the total chip area over which the horizontal grinding force acts decreases.

In the case of the diamond wheel, the horizontal grinding force is low and independent of the rate of material removal. Material is removed by a brittle fracture, and thus the specific grinding energy is a measure of the stress to initiate and propagate cleavage cracks.

The difference in vertical grinding forces, noted in figs. 1 to 4, between the alumina and diamond wheels is also consistent with the different mechanisms of material removal. Under the conditions of climb grinding employed in this study, the chips formed at the leading edge of the wheel-workpiece interface must travel between the wheel and the workpiece. At low rates of material removal, the chips are expelled efficiently and the vertical grinding forces are low. As the rate of material removal increases, the vertical grinding forces increase drastically. In the case of the aluminium wheel, the chips are sheared plastically and resemble the ideal triangular chip shape assumed in fig. 5 and illustrated schematically in fig. 9. With the diamond wheel, the large block-shaped chips are forced between the closed structure diamond wheel and the workpiece causing much higher grinding forces at high

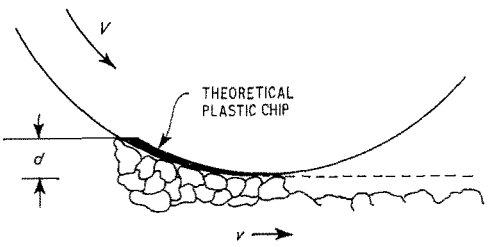

Figure 9 Schematic diagram showing possible differences in mechanism of chip formation under a 46-grit alumina wheel and a 100-grit diamond wheel; the plastic chip is formed by the alumina wheel.

removal rates. This is also illustrated schematically in fig. 9.

4.6. Effects of Crystal Orientation

If the above interpretation is correct, i.e. that the horizontal grinding forces measured with the alumina wheel are proportional to the stress to induce plasticity in a chip during machining, then it is to be expected that there will be a sensitivity to crystallographic orientation. This sensitivity is illustrated very nicely by the results of fig. 3.

The relative deformability of magnesium oxide crystals with orientation can be inferred from the resolved shear stress over the slip planes. In terms of the applied stress, σ, the shear stress, τ, resolved over $\{1\,1\,0\}$ planes in $\langle 1\,1\,0\rangle$ directions is given by [14]

$$\tau = \sigma \cos\lambda \cos\phi \qquad (12)$$

where λ is the angle between the grinding direction and the $\{1\,1\,0\}$ slip plane normal, and ϕ is the angle between the grinding direction and the $\langle 1\,1\,0\rangle$ slip direction. In fig. 10, the resolved shear stress factor, $\cos\lambda\cos\phi$, is plotted as a function of the angle between the grinding direction and [1 0 0] for the four most highly stressed slip systems in magnesium oxide. The grinding force curves shown in fig. 3 are similar to the inverse of those shown in fig. 10. The variation in grinding forces with crystal orientation, therefore, is related to the ability of the workpiece to undergo plastic deformation. The ideal situation for grinding with the alumina wheel is over the $\{1\,0\,0\}$ face in the $\langle 1\,0\,0\rangle$ direction, since two slip systems are then favourably oriented for the maximum shear stress as indicated by fig. 10. This agrees with experimental observation. If the orientation deviates too far from ideal, the grinding forces become excessive and the material shatters.

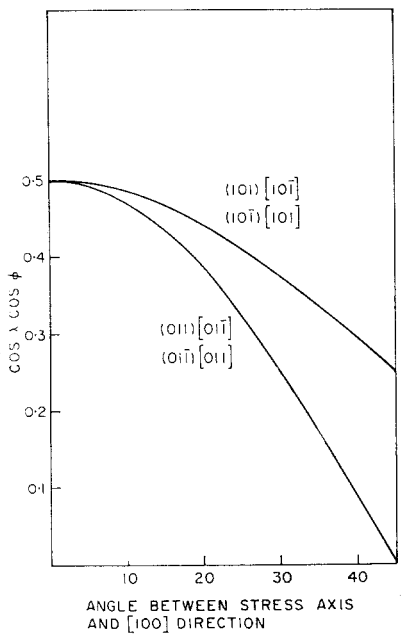

Figure 10 Resolved shear stress factor plotted as a function of the angle between the stress axis (the grinding direction) and the [100] direction for crystals ground on (001) faces.

The horizontal grinding forces measured with the diamond wheel are not sensitive to orientation. This is again consistent with the conclusion that plastic shear is not involved in chip formation for this particular wheel-workpiece configuration. A subsurface deformed layer is still observed [4], of course, but this is due to the propagation of dislocations under the influence of the short range stress field existing at the leading edge of the wheel-workpiece interface.

5. Conclusions

The above results and discussion have shown that:
(i) Grinding forces are sensitive to the events occurring at the wheel-workpiece interface during the machining of ceramics.
(ii) Grinding force dependence on material removal rate can be used to distinguish different mechanisms of material removal.
(iii) Grinding forces can be rationalised to yield an expression for the stress acting on a chip. These stresses are very high and approach the theoretical strength.
(iv) If the material is removed by plastic flow, the grinding forces show a dependence on orientation consistent with the variation in resolved shear stress over active slip systems.

Acknowledgements

The authors are indebted to D. Woodward for able experimental assistance during the course of this research. The continued interest of Dr C. H. Li, Director, Honeywell Corporate Research Center, and Dr A. Diness, Office of Naval Research, is gratefully acknowledged. This work was supported by the Office of Naval Research.

References

1. "Proceedings of a Symposium on the Science of Ceramic Machining and Surface Finishing", edited by S. Schneider (Nat. Bur. Standards, 1970) to be published.
2. "Ceramic Processing", Publication 1576 (National Academy of Sciences, Washington, DC, 1968), p. 145.
3. B. G. KOPEKE and R. J. STOKES, *J. Mater. Sci.* **5** (1970) 240.
4. B. G. KOPEKE, in Reference 1.
5. R. J. STOKES, in Reference 1.
6. P. J. GIELISSE and J. STANISLAO, in Reference 1.
7. E. R. MARSHALL and M. C. SHAW, *Trans. Amer. Soc. Mech. Eng.* **74** (1952) 51.
8. W. R. BACKER, E. R. MARSHALL, and M. C. SHAW, *ibid* **74** (1952) 61.
9. W. R. BACKER and M. E. MERCHANT, *ibid* **80** (1958) 141.
10. G. S. REICHENBACH, J. E. MAYER, S. KALPAKCIOGLU, and M. C. SHAW, *Trans. Amer. Soc. Mech. Eng.* **78** (1956) 847.
11. W. R. BACKER, discussion to Reference 11, *ibid*, 857.
12. F. A. MCCLINTOCK and A. S. ARGON, "Mechanical Behaviour of Materials", (Addison-Wesley, Massachusetts, 1966) p. 118.
13. J. F. BELL, "The Physics of Large Deformation of Crystalline Solids", (Springer-Verlag, New York, 1968).
14. F. P. BOWDEN and C. A. BROOKES, *Proc. Roy. Soc.* **295A** (1966) 244.

Received 8 October and accepted 12 October 1971.